



An Application of a 3-RRRS 6 DOF Parallel Manipulator

Anirudh RV, Sai Krishna A, Kulothungan S and Dr. Anjan Kumar Dash*

1School of Mechanical Engineering, SASTRA Deemed to be University, Thanjavur, India

(Received 3 November 2018; Accepted 10 January 2019; Published on line 1 June 2020)

*Corresponding author: anjandash@mech.sastra.edu

DOI: 10.5875/ausmt.v10i1.2048

Abstract: A new drive simulator is designed and fabricated through three legged, 6-DOF 3-RRRS (Revolute- Revolute- Revolute- Spherical) parallel manipulator having three 1-DOF joints which are of revolute type and the middle joint being passive. The three legs are placed equilaterally on the base. Base joint rotates about a vertical axis whereas the other two joints rotate parallel to horizontal plane. The main objective of this drive simulator is to reduce the overall cost of a drive simulator which is done by replacing the conventional drive simulators having linear actuators with ones having rotatory actuators. Conventional drive simulators are 6 legged and each actuator is a linear actuator. The proposed design of drive simulator is having 3 legs which leads to increase in workspace and since prismatic actuators are replaced by rotary actuators the overall cost is also reduced. For the proposed drive simulator, inverse kinematics model is generated in a closed form way and workspace of the fabricated drive simulator is verified and workspace volume is calculated for all possible orientations and plotted. Kinematic control is done through Arduino based on inverse kinematics model.

Keywords: Drive Simulator; Parallel manipulator; spatial manipulator; Inverse kinematics; Workspace.

I. INTRODUCTION

Drive simulators are basically used as a training equipment for drivers to help them in their learning process. They also find their application in entertainment parks and various other vehicle testing centres. These simulators simulate the required road conditions and help monitor the behaviour, performance and attention of the driver. They are also used to evaluate new vehicle designs and assistance systems.

Most of the existing drive simulators are based on the Stewart platform, the most common 6-DOF parallel manipulator [1,2]. Most of the famous drive simulators made by Daimler-Benz, Ford, BMW etc are all based on 6-DOF hexapod [2]. However, the cost of the hexapod with 6 linear actuators is very high and if they are all hydraulic actuators then additional cost makes it un-economical.

This article presents an alternative design to drive

simulator. Of the 6-DOF parallel manipulators, the 3-legged parallel manipulators are not much researched [4,5,6]. Of these, the 3-RRRS, 6-DOF parallel manipulator has the topology to be an alternative design for drive simulator. In this article, this topology is taken to verify its ability to be an alternative design for drive simulator.

The solid model of this alternative design based on 3-RRRS 6-DOF topology is presented in Fig. 1. This manipulator has a mobile platform whose movement is controlled by a set of links connected serially with the base platform. Starting from base platform, there are three rotary joints out of which any two can be active and the other one can be passive and it connects the mobile platform with a spherical joint. Thus each leg has two rotary actuators and one passive joint. This gives the following major advantages with respect to 6-DOF Stewart platforms [7,8]

- Decoupled kinematics- This means, for example, to move the mobile platform along Z-axis, only the three distal motors are to be operated. The same advantage is there for all other degrees of freedom

also. But in case of Stewart platform, to move the end-effector along any axis, all 6 actuators are to be operated.

- This also makes inverse kinematics very easy and so also controlling of the manipulator.
- Since there are three legs, the workspace of such a topology becomes larger compared to that of a Stewart platform because the workspace becomes the intersection of 3 spheres rather than 6 spheres as in the case Figure 1: Drive simulator modelled using SolidWorks 2016 of Stewart platform.
- The cost of the manipulator also reduces significantly because there is no linear actuator.

Considering all these advantages, this article proposes an alternative design to drive simulator based on the 3-RRRS topology. In this article, the design is proposed, inverse kinematics model is developed in a closed form way, workspace and singularity analysis is performed and kinematic control is also implemented.

II. DESIGN AND FABRICATION OF DRIVE SIMULATOR

A. Design of manipulator

As mentioned above, the proposed 3-RRRS 6-DOF parallel manipulator has three legs each having 6 DOFs. The axis of the base joint is normal to the base platform and to carry the vertical load a long bearing is provided at the base. The other two joints of each leg have axes parallel to each other and parallel to the base platform. Out of these, the distal rotary joint is made active because of singularity consideration which is discussed in the next sub-section. A 3-DOF spherical joint connects the leg with the mobile platform. Following

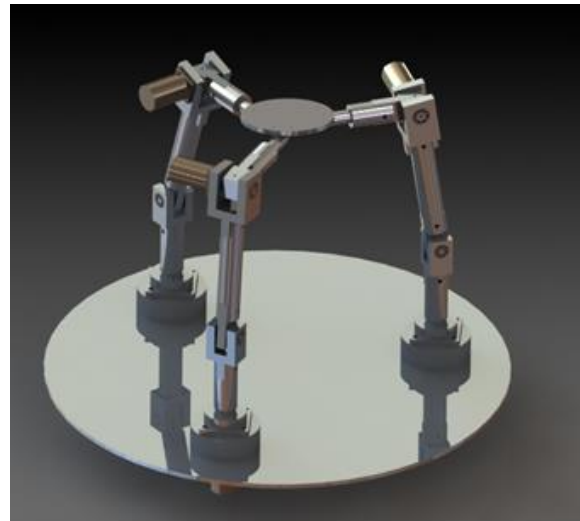


Figure 1. SolidWorks model describes the proposed drive simulator.

B. Singularity analysis-placement of actuators

Since the number of legs are reduced to 3, it necessitates to place the 6 actuators in 3 legs. To have a symmetric actuation scheme, 2 actuators are placed in each leg. In each leg there are three rotary joints and finally there is a spherical joint which connects each leg to the mobile platform. So now it reduced to the option of placing the two actuators in any two of the three rotary joints, i.e., the actuators can be placed in 1st and 2nd joints, 2nd and 3rd joints or 1st and 3rd joints. Let us discuss each of these cases one by one.

Placement of actuators at 1st and 2nd joints:

By this actuation scheme, 1st and 2nd joints of each leg are active and the 3rd joint becomes a passive joint. Based on [9], it is understood that such 3-RRRS parallel manipulators have a passive joint plain and in that plain, there are hundreds of singularities. Passive joint plane is described as the plane made out of the position of the three passive joints at zero orientation. This is briefly explained below. The corresponding Jacobian matrices for 1-2 actuation scheme are as follows:

$$AV_e = B\dot{q} \quad \text{where}$$

$$A = \begin{bmatrix} a_{11} \\ a_{12} \\ a_{21} \\ a_{22} \\ a_{31} \\ a_{32} \end{bmatrix}$$

where

Dr Anjan Kumar Dash received his PhD from NTU, Singapore and he has wide knowledge in parallel manipulators and its various applications. He has developed algorithms for singularity avoidance for 3-RRRS 6 DOF parallel manipulators, workspace analysis, and optimization. In a funded project, Dr Dash has proved the applicability of a 3-RRRS parallel manipulator as a 6-DOF shake table. He also takes keen interest in design and development of other parallel manipulators-like 3-RRR, 3-PRR etc. He is also working on application of mechanisms for rehabilitation purpose and developed prototype walking aids for paraplegic patients. He is also developing a mechanism for developing a portable RO plant which can be useful for expeditioners. He is also a member of IEEE society.

Email addresses

Sl No	Name	Email
1	Anirudh RV	rvanirudh97@gmail.com
2	Sai Krishna A	krisdysai@gmail.com
3	Kulothungan S	realkulothungan@gmail.com
4	Dr. Anjan Kumar Dash	anjandash@mech.sastra.edu

$$\begin{aligned}
 a_{11} &= \{([I - \hat{p}_{14}]s_{12}) \times ([I - \hat{p}_{14}]s_{13}) - \{([I - \hat{p}_{14}]s_{12}) \times ([I - \hat{p}_{14}]s_{13}) \times p_{14}\}^T \\
 a_{12} &= \{([I - \hat{p}_{24}]s_{21}) \times ([I - \hat{p}_{24}]s_{23}) - \{([I - \hat{p}_{24}]s_{21}) \times ([I - \hat{p}_{24}]s_{23}) \times p_{24}\}^T \\
 a_{21} &= \{([I - \hat{p}_{24}]s_{22}) \times ([I - \hat{p}_{24}]s_{23}) - \{([I - \hat{p}_{24}]s_{22}) \times ([I - \hat{p}_{24}]s_{23}) \times p_{24}\}^T \\
 a_{22} &= \{([I - \hat{p}_{24}]s_{21}) \times ([I - \hat{p}_{24}]s_{23}) - \{([I - \hat{p}_{24}]s_{21}) \times ([I - \hat{p}_{24}]s_{23}) \times p_{24}\}^T \\
 a_{31} &= \{([I - \hat{p}_{34}]s_{32}) \times ([I - \hat{p}_{34}]s_{33}) - \{([I - \hat{p}_{34}]s_{32}) \times ([I - \hat{p}_{34}]s_{33}) \times p_{34}\}^T \\
 a_{32} &= \{([I - \hat{p}_{34}]s_{31}) \times ([I - \hat{p}_{34}]s_{33}) - \{([I - \hat{p}_{34}]s_{31}) \times ([I - \hat{p}_{34}]s_{33}) \times p_{34}\}^T
 \end{aligned}$$

and $B = \text{diag}\{b_{11}, b_{12}, b_{21}, b_{22}, b_{31}, b_{32}\}$ where b_{ij} are the scalar elements.

Here p_{i4} is the position vector joining the origin of base frame to the end point of i^{th} leg, s_{ij} is the twist of the j^{th} ($j = 1, 2$) joint of the i^{th} leg and \hat{p}_{i4} is the cross product matrix corresponding to the vector p_{i4} . Forward and inverse singularity points can be easily obtained by equating the determinants of the matrices A and B to zero respectively. Since inverse singularity points lie at the boundary of the workspace, they are of less danger than the forward singularity points which lie inside the boundary. By equating the determinant of the matrix A to zero, one gets the forward singularity points. It can be seen from [9] that for 1-2 actuation scheme, the forward singularity points mostly lie on the passive joint plane. At zero orientation, almost all the points in this plane are singular points (Fig.3).

passive joint plane is made out of the 3 passive joints of the three legs at zero orientation. From this it can be estimated how dangerous and how crucial is the location of the passive joint in these manipulators.

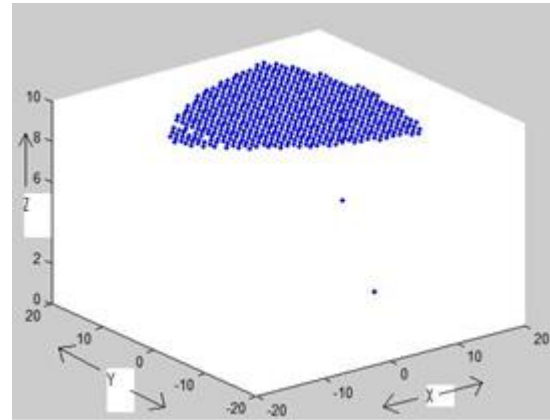


Figure 3: Location of the singularities for 1-2 actuation scheme

Placement of actuators at 1st and 3rd joints:

For 1-3 actuation scheme, the Jacobian matrices will change because the placement of the actuators affect the Jacobian matrices. The new Jacobian matrices are as follows:

$$AV_e = B\dot{q} \quad \text{where}$$

where

$$A = \begin{bmatrix} a_{11} \\ a_{13} \\ a_{21} \\ a_{23} \\ a_{31} \\ a_{33} \end{bmatrix}$$

$$\begin{aligned}
 a_{11} &= \{([I - \hat{p}_{14}]s_{12}) \times ([I - p_{14}]s_{13}) - \{([I - \hat{p}_{14}]s_{12}) \times ([I - p_{14}]s_{13}) \times p_{14}\}^T \\
 a_{13} &= \{([I - \hat{p}_{14}]s_{11}) \times ([I - p_{14}]s_{12}) - \{([I - \hat{p}_{14}]s_{11}) \times ([I - p_{14}]s_{12}) \times p_{14}\}^T \\
 a_{21} &= \{([I - \hat{p}_{24}]s_{22}) \times ([I - p_{24}]s_{23}) - \{([I - \hat{p}_{24}]s_{22}) \times ([I - p_{24}]s_{23}) \times p_{24}\}^T \\
 a_{23} &= \{([I - \hat{p}_{24}]s_{21}) \times ([I - p_{24}]s_{22}) - \{([I - \hat{p}_{24}]s_{21}) \times ([I - p_{24}]s_{22}) \times p_{24}\}^T \\
 a_{31} &= \{([I - \hat{p}_{34}]s_{32}) \times ([I - p_{34}]s_{33}) - \{([I - \hat{p}_{34}]s_{32}) \times ([I - p_{34}]s_{33}) \times p_{34}\}^T \\
 a_{33} &= \{([I - \hat{p}_{34}]s_{31}) \times ([I - p_{34}]s_{32}) - \{([I - \hat{p}_{34}]s_{31}) \times ([I - p_{34}]s_{32}) \times p_{34}\}^T
 \end{aligned}$$

and $B = \text{diag}\{b_{11}, b_{13}, b_{21}, b_{23}, b_{31}, b_{33}\}$ where b_{ij} are the scalar elements.

For such a configuration, the passive joint plane will lie at a distance of l_1 from the base and most of the singularities will lie in this plane.

Comparing the above two actuation schemes, it can be concluded that singularities lie at a distance of l_1 from the base for 1-3 actuation scheme; thus beyond l_1 till

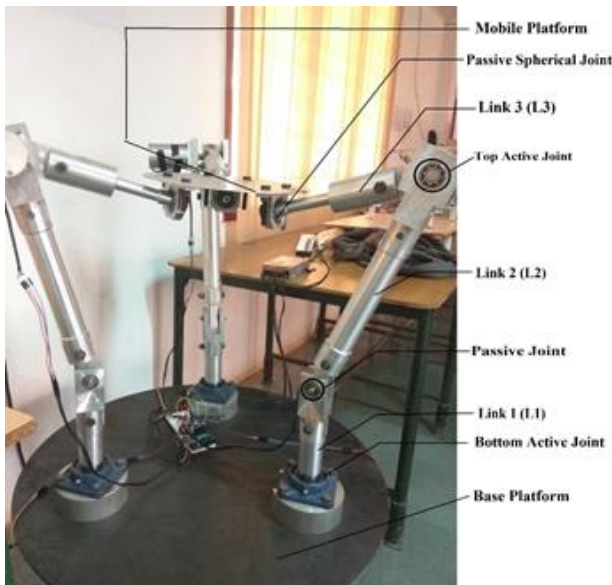


Figure 2. Fabricated and assembled view of Drive Simulator

Figure 2 shows the fabricated and assembled view of the manipulator. If 1-2 actuation scheme is implemented, in which case inertia mass will be less, the passive joint plane will lie at a height of $l_1 + l_2$ because third joint is the passive joint. The singularity distribution is shown as below in Fig. 3. In this figure, all the blue dots are singular points and it can be seen that they constitute a plane. This plane is called the passive joint plane. The

approximate height of $l_1+l_2+l_3$, the workspace is without any singularity and is available for movement of the end-effector. On the other hand, for 1-2 actuation scheme, passive joint plane lies at a height of l_1+l_2 . By this location at the middle of the workspace, the entire workspace becomes unusable. That is, although the space below and above l_1+l_2 is free of singularities, since the singularities are located in between the workspace, it makes the entire workspace unusable. So, based on this singularity consideration, 1-3 actuation is preferable compared to 1-2 actuation scheme although there is more inertia mass in case of 1-3 actuation scheme. To address the issue of more inertia mass in case of 1-3 actuation scheme, mass of the mobile platform, mass of the 3rd link and spherical joint are minimized as much as possible. Also, the torque rating of the actuator at the third joint is less compared to that of the base. This makes the actuator less weight.

Placement of actuators at 2nd and 3rd joints:

This is not at all a good design because the mass in motion will be too much.

So considering both the criterion -location of singularities and mass in motion, it can be concluded that 1-3 actuation with less masses of 3rd link, mobile platform, spherical joint, and 2nd actuator is the optimal solution.

C. Fabrication of Drive simulator

The fabrication is carried out in robust CNC (Computer Numerical Control) machines. Aluminum alloy 6061 is made use in fabricating links. Aluminum offers greater weight reduction compared to other materials without compromising strength and functionality. Moreover, aluminum is corrosive resistant and has great mechanical properties that include machinability and strength. The main reason to choose this grade of aluminum is its availability and its low cost.

The fabrication is done meticulously to avoid addition weights in links that would increase the effort of the actuators (Servo motors) to move accurately. Extremities would be that it might also cause the actuators to fail which will be too exorbitant to afford. So the links are made hollow without any loss in mechanical strength and functionality.

III. INVERSE KINEMATICS

Inverse kinematics is the process of obtaining the joint angles/displacements so that the end effector is mapped to required position and orientation.

A. Methodology

Geometrical method is used to find the joint angles for the given position and orientation which gives closed form solution for the inverse kinematics. This method is adopted as the construction of the drive simulator is simple and doesn't need complex inverse kinematics calculations. This reduces the complexity.

Let the point where first leg of the drive simulator meets the base plate be the inertial frame of reference. Initially the home position of the end effector is set and the values of home position is noted in terms of position and orientation along all 3 axes. Any further movement of end effector is calculated from the home position only.

The calculation of 9 angles i.e. three base motor rotation angles, three passive joint angles, three top motor angles is carried out in a geometrical method as described below.

For example, the calculation of 9 angles for a small displacement along X-axis is shown below (Fig. 4).

1) Angles for the first leg:

a) Base motor angle:

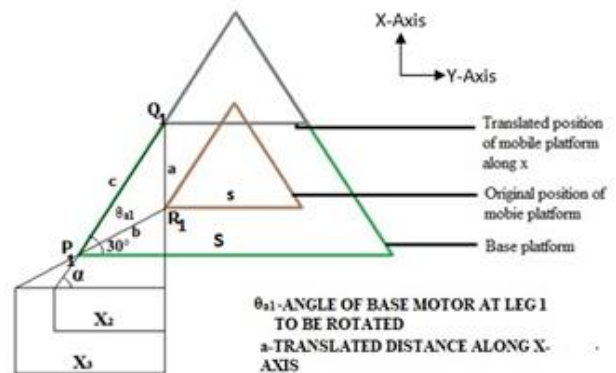


Figure 4: Top view of leg 1 of 3-RRRS type 6-DOF parallel manipulator

Let the end effector be translated through a distance 'a' units along X-axis (as shown in the top view-Fig.4).

The distance 'b' between two vertices is given by,

$$b = \frac{S - s}{\sqrt{3}} \tag{2}$$

where 'S' is the side length of base and 's' is the side length of the end effector.

Applying cosine law to the triangle $P_1Q_1R_1$,

$$c = \sqrt{b^2 + a^2 - 2bc \cos \angle P_1R_1Q_1} \tag{3}$$

Here $\angle P_1R_1Q_1$ is 120°. With above value of 'c', θ_{a1} can be calculated using sine law (Fig.4).

$$\theta_{a1} = \sin^{-1} \left(\frac{a \times \sin \angle P_1R_1Q_1}{c} \right) \tag{4}$$

b) Top motor angle:

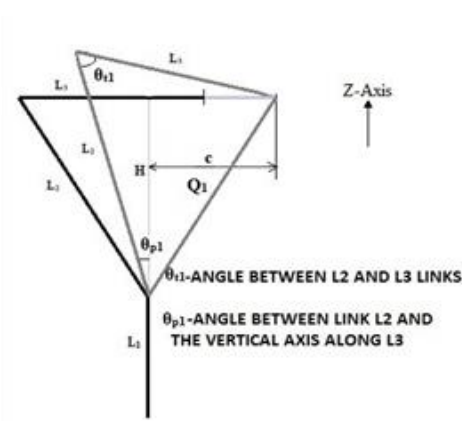


Figure 5: Front view of leg 1 of 3-RRRS 6-DOF parallel manipulator

From Fig. 5,

$$Q_1 = \sqrt{H^2 + c^2} \tag{5}$$
 where Q_1 is the distance between the 2nd joint and the spherical joint of the leg, 'H' is the vertical distance along Z-axis of the end effector i.e. home position.

Applying cosine law to find θ_{t1} ,

$$\theta_{t1} = \text{Cos}^{-1} \left(\frac{L_2^2 + L_3^2 - Q_1}{2 \times L_2 \times L_3} \right) \tag{6}$$

Passive Joint angle:

Similarly, to find θ_{p1} , sine law is applied in Figure 4.

$$\theta_{p1} = \text{Sin}^{-1} \left(\frac{L_3 \times \text{Sin} \theta_{t1}}{Q_1} \right) - \text{Sin}^{-1} \left(\frac{c}{Q_1} \right) \tag{7}$$

2) Angles for the second leg:

a) Base motor angle (Fig. 6):

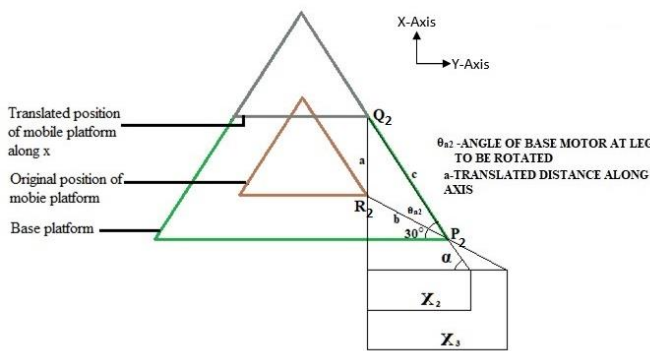


Figure 6: Base motor rotation in leg 2

As done in case of leg-1, adopting similar method,

$$\theta_{a2} = \text{Sin}^{-1} \left(\frac{a \times \text{Sin} \angle P_2 R_2 Q_2}{c} \right)$$

b) Top motor angle (Fig.7):

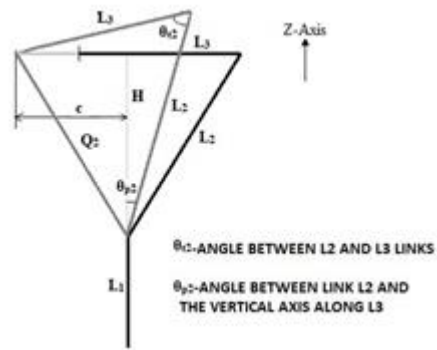


Figure 7: Front view of leg 2

$$Q_2 = \sqrt{H^2 + c^2} \text{ and}$$

$$\theta_{t2} = \text{Cos}^{-1} \left(\frac{L_2^2 + L_3^2 - Q_2}{2 \times L_2 \times L_3} \right)$$

c) Passive joint angles:

Following the same procedure as above,

$$\theta_{p2} = \text{Sin}^{-1} \left(\frac{L_3 \times \text{Sin} \theta_{t2}}{Q_2} \right) - \text{Sin}^{-1} \left(\frac{c}{Q_2} \right)$$

3) Angles for third leg:

a) Base motor angle:

There is no rotation observed at the base motor of the third leg, as there is only translation along X-axis. Only the top motor angle and the passive angle change in this case.

b) Top motor angle:

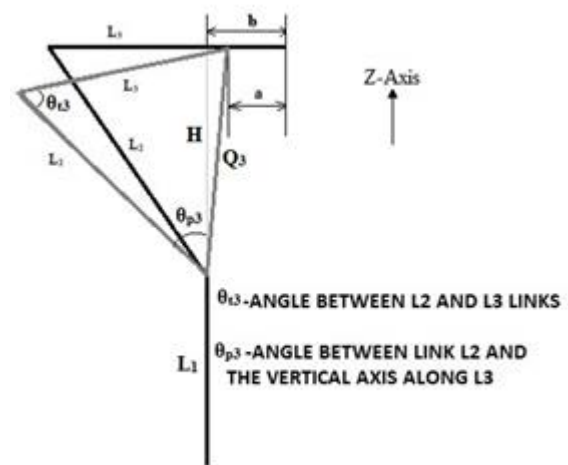


Figure 8 Front view of leg 3

This calculation is bit different for this leg as the other two legs move forward to accomplish movement

along positive X-axis. So that this leg has to retract backwards the same amount (Fig. 8).

Hence the value of Q3 is calculated as,

$$Q_3 = \sqrt{(b-c)^2 + h^2} \tag{8}$$

The remaining calculation remains same and is performed using cosine law to find out the top motor angle (θ_{t3}).

c) *Passive angle*

$$\theta_{p3} = \text{Sin}^{-1}\left(\frac{L_3 \times \text{Sin} \theta_{t2}}{Q_3}\right) - \text{Sin}^{-1}\left(\frac{c}{Q_3}\right)$$

IV. WORKSPACE DETERMINATION

Workspace is said to be defined as a space in 3D within which the end effector of the manipulator can traverse ensuring all 6 DOF without any loss in stability. However, it is well known that a parallel manipulator has limited workspace because of complex kinematic singularities [7,8,9]. Methods available to determine the workspace of parallel manipulators are discretization method, geometric method and numerical algorithm [10]. In this paper, discretization method is used because as mentioned and adopted in [11,12], discretization method makes use of the inverse kinematics of parallel manipulator which is easier compared to the forward kinematics. Also, by making a finer discretization, better resolution of the workspace can be obtained.

A. Methodology

In this paper, discretization method is followed to determine the workspace. Inverse kinematics is applied at each of these discretized points to determine whether that point is within the workspace or not.

The plot obtained is an intersection of three spheres. In the obtained plot green filled dots denotes the points in reachable workspace. Figures 9 and 10 are the two views of the workspace at zero orientation.

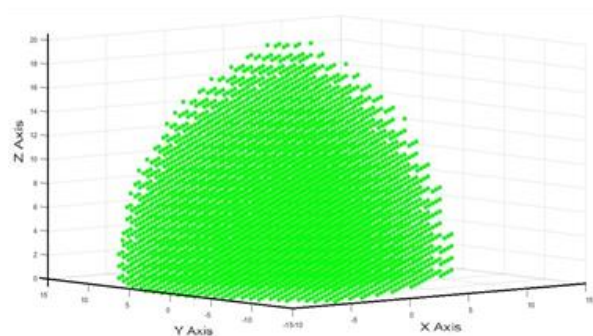


Figure 9: Accessible workspace of drive simulator (View 1)

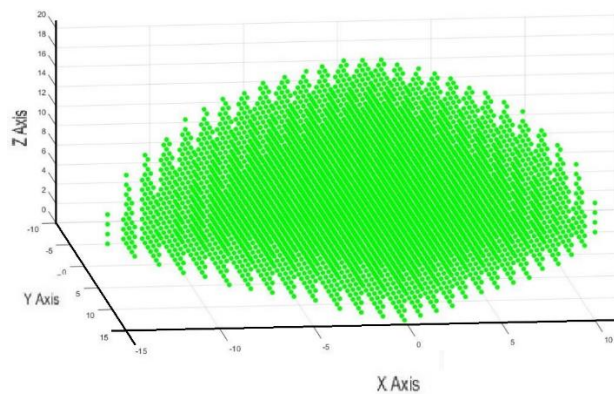


Figure 10: Accessible workspace of drive simulator (View 2)

B. Workspace volume determination and analysis

For determination of the volume of the workspace, each point of the workspace is considered to represent unit cube volume. So the number of points that exist in the workspace, that much unit cube of volume the workspace has. Thus the volume of the workspace is calculated while the points for the workspace is being plotted. The points that have feasible position and orientation are summed up to find the workspace volume. Usually the workspace volume is determined in cubic cm here.

When workspace volume is calculated in cm³ for the required orientation, it is seen that the reachable workspace volume differs for various orientations. The reachable workspace volume actually reduces for even a small change in orientation about any direction.

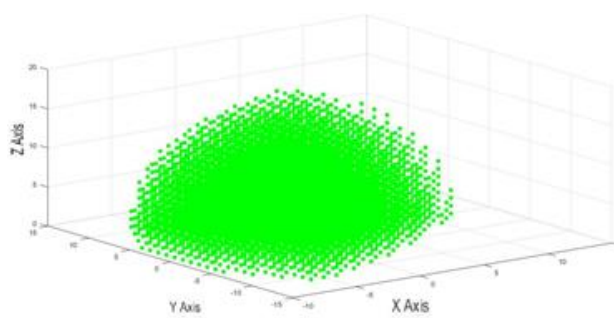


Figure 11: Accessible workspace when the drive simulator is rotated by 15° about Z-axis

When the drive simulator is rotated 15° about Z-Axis the workspace volume is reduced from 5022 cm³ to 3707 cm³ as shown in Fig. 11.

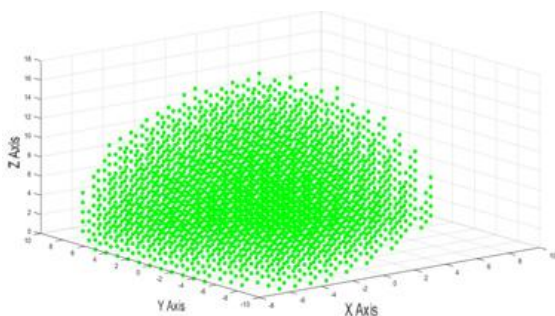


Figure 12: Accessible workspace when the drive simulator is rotated by 25° about Z-axis

Further when the drive simulator is rotated 25° about Z-Axis the workspace volume is reduced from 5022 cm³ to 2602 cm³ as shown in Fig. 12.

V. CONTROL OF DRIVE SIMULATOR

The basic control of the drive simulator achieved through 6-DOF 3-RRRS manipulator is done using the high-torque DC servo motor with built-in optical encoder. A High torque motor is needed since the manipulator is heavy and the normal torque motors fail to lift the setup. A total of 6 high torque servo motors are used with 3 motors positioned at the bottom and 3 at the top.

In a single set of links the individual links are connected by totally 4 joints:

- R-Active rotary joint powered by DC servo
- R-Passive rotary joint
- R-Active rotary joint powered by DC servo
- S-Passive spherical joint through a double row spherical bearing.

A. Actuator requirements

Servo motor RMCS 2201 with a torque of 120kgcm and speed 10RPM is used as the rotary actuators. The motor has a built-in encoder with a resolution 0.2° and a driver. Hence a less complex circuit is likely to be obtained in the assembly. It can possibly be controlled by 4 methods

- Green- V+ (Input power supply from 11V DC to 15V DC)
- Black- GND (Ground)
- Yellow-UART RXD (Receive data)
- Orange-UART TXD (Transmit data)
- Red- SDA (Serial Data)
- Brown-SCL(Serial Clock)

B. Available Control Methods

To control the speed and motion of the RMCS-2201 DC servo motor there are four widely used methods. Among these four methods provided by the manufacturer any one suitable and viable method can be opted. The methods are explained below:

- Position and speed control using UART
- Position and speed control using I2C method
- Speed control using Analog input
- Position control using PPM signal

C. Adopted method of control- UART

UART (Universal Asynchronous Receiver-Transmitter) is the method made use to control the actuators. This method is found to be highly facile and easy to employ.

The ideal way to use the UART interface of the RMCS-2201 is with a terminal software like Putty and Arduino environment. It works at a fixed baud rate of 9600bps. It prompts the user to enter the decimal value and string value in the environment. The value of a variable given by the user must provide an integer decimal. The decimal value denotes the quantity of rotation, its positive or negative sign denotes the direction of the resulting movement and the string denotes the action for which the value is specified. For example, to rotate through 90° clockwise direction with respect to current position, input is 'R450' which is to be written in the serial window of the Arduino IDE. The decimal value is calculated as follows:

$$\frac{\text{Angle_required}}{0.2} = \text{Integer_value} \quad \text{i.e.} \quad \frac{90}{0.2} = 450$$

Here 0.2 is the resolution of the optical encoder of the actuator. Now the actuator moves 450 steps to cover 90°. Now R450 denotes rotation through 90° clockwise. For counter-clockwise rotation input is R-450.

A microcontroller controls all 6 actuators that are powered through an Switched Mode Power Supply (SMPS). The microcontroller sends the signals in-terms of commands to the UART through RXD terminal of the motor and reads the feedback from TXD port of the motor as shown in Fig. 13.

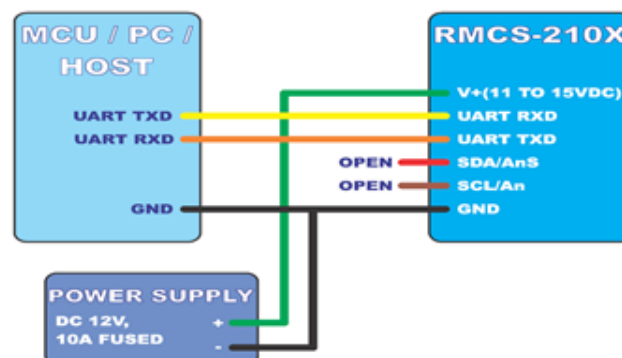


Figure 13: Interfacing Diagram for UART method of control

Table 1: List of the available command code

Command	Description	Value Minimum	Value Maximum
'S'	Read/Write Motor Speed and Direction	-255	+255
'M'	Read/Write Motor Max Speed	0	255
'D'	Read/Write Speed Damping	0	255
'E'	Read/Write I2C address	0	127
'Y'	Load Default Values of all settings and gains	-	-
'P'	Read/Write Encoder Position	-2147483648	2147483647
'G'	Read/Write Go to Position Command	-2147483648	2147483647
'R'	Write Relative Go to Position Command	-2147483648	2147483647
'A'	Read/Write Speed-Feedback Gain term	0	32767
'B'	Read/Write P-Gain term	0	32767
'C'	Read/Write I-Gain term	0	32767
'X'	Auto-calibrate Speed-Feedback Gain term	-	-

List of available command codes are as shown in Table-1.

D. Wiring Setup

Driving the normal DC servo motor is highly different from the high torque motors since the control mechanism and the power requirements are very different in the high-end motors. In the RMCS-2201 motor, it has various number of pins and has different controlling mechanism available to control the motor. Hence any suitable option can be opted to actuate the motor.

The plausible solution reduces complexity and time for debugging errors, if in case any. The wires to any motor are bunched together so that it can be easily plugged and removed. The positives and negatives are grouped to connect seamlessly to the power supply. The wiring setup includes power supply from SMPS which supplies 12V DC and 7.5 A for each motor to positive terminal of the motor. The top motors and bottom motors terminals are separated and are connected in breadboard. The negative terminals are pooled together and a common negative terminal is grounded with the ground terminal of the Arduino. The TXD and RXD ports are connected in the Arduino digital ports. Due to limited hardware serial ports, software serial is employed. Using software serial the digital pins of the microcontroller are assigned to do the task of the serial ports [N]. Hence all six motors are controlled seamlessly using a single microcontroller as shown in Fig. 14 and Fig. 15.

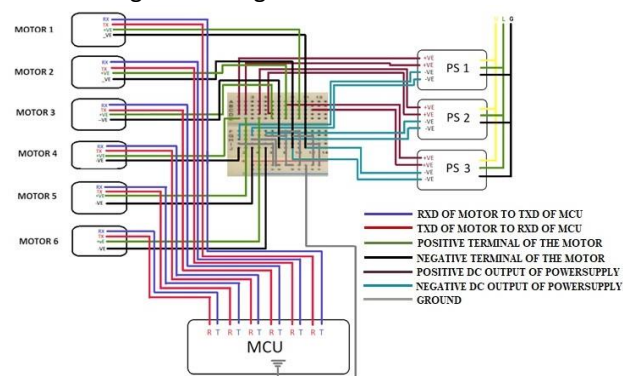


Figure 14: Interfacing all six motors with microcontroller with powersupply

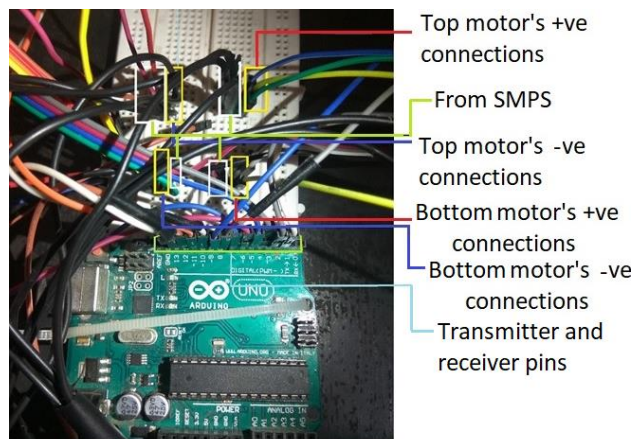


Figure 15: Wiring setup of motors with the microcontroller


VI. ACKNOWLEDGMENT

This project is supported by Innovation Fund, SASTRA Deemed University (2017-18), Tamil Nadu, India.

References

- [1] E. Balana, "A Survey Of Driving Research Simulators Around The World, Institute Of Transport Studies,"University Of Leeds, Leeds, UK, 1996.
- [2] J. J. Slob, "State-of-the-Art Driving Simulators, a Literature Survey", Department Mechanical Engineering Control Systems Technology Group, Eindhoven University of Technology, Netherlands, 2008.
- [3] K. Dash, "Kinematic Design of Reconfigurable Parallel Manipulators", Ph.D. dissertation, Nanyang Technological University, Singapore, 2002.
- [4] K. Dash, I.-M. Chen, S. H. Yeo, and G. Yang, "Instantaneous kinematics and singularity analysis of three-legged parallel manipulators," *Robotica*, vol. 22 (2), pp. 189-203, 2004 doi: [10.1017/s0263574703005496](https://doi.org/10.1017/s0263574703005496)
- [5] K. Dash, S. H. Yeo, G. Yang, and I.-M. Chen, "Workspace analysis and singularity representation of three-legged parallel manipulators," in proceeding of *7th International Conference on Control, Automation, Robotics and Vision*, Singapore, Dec 2-5, 2002, pp. 962-967 2002. doi: [10.1109/icarcv.2002.1238554](https://doi.org/10.1109/icarcv.2002.1238554)
- [6] J. Angeles, G. Yang, and I. M. Chen, "Singularity analysis of three-legged, six-DOF platform manipulators with RRRS legs," in proceeding of *2001 IEEE/ASME International Conference on Advanced Intelligent Mechatronics*, July 8-12,

- 2001, Italy, pp. 32-36.
doi: [10.1109/aim.2001.936426](https://doi.org/10.1109/aim.2001.936426)
- [7] B. Pham, S. H. Yeo, G. Yang, M. S. Kurbanhusen, and I.-M. Chen, "Force-closure workspace analysis of cable-driven parallel mechanisms", *Mechanism and Machine Theory*, vol.41(1), pp. 53-69, 2006.
doi: [10.1016/j.mechmachtheory.2005.04.003](https://doi.org/10.1016/j.mechmachtheory.2005.04.003)
- [8] B. Pham, S. H. Yeo, and Y. Guilin, "Workspace analysis and optimal design of cable-driven planar parallel manipulators", in proceeding of *IEEE Conference on Robotics, Automation and Mechatronics*, December 1-3, 2004, pp. 219–224.
doi: [10.1109/ramech.2004.1438920](https://doi.org/10.1109/ramech.2004.1438920)
- [9] J. W. Yoon, J. Ryu, and Y.-K. Hwang, "Optimum design of 6-DOF parallel manipulator with translational/rotational workspaces for haptic device application", *Journal of Mechanical Science and Technology*, vol. 24(5), pp. 1151-1162, 2010.
doi: [10.1007/s12206-010-0321-8](https://doi.org/10.1007/s12206-010-0321-8)
- [10] K. Dash, I.-M. Chen, S. H. Yeo, and G. Yang, "Workspace generation and planning singularity-free path for parallel manipulators", *Mechanism and Machine Theory*, vol. 40(7), pp. 776-805, 2005.
doi: [10.1016/j.mechmachtheory.2005.01.001](https://doi.org/10.1016/j.mechmachtheory.2005.01.001)
- [11] Gosselin, "Determination of the workspace of 6-dof parallel manipulators", *Journal of Mechanical Design*, vol. 112(3), pp. 331-336, 1990.
doi: [10.1115/1.2912612](https://doi.org/10.1115/1.2912612)
- [12] J. P. Merlet, *Parallel Robots*. Springer Science and Business Media, 2012.

 ©The Authors. This work is licensed under the Creative Commons Attribution-NonCommercial-NoDerivatives 4.0 International License.